

MIT Open Access Articles

*The Impenetrable Barrier: Suppression of
Chorus Wave Growth by VLF Transmitters*

The MIT Faculty has made this article openly available. **Please share**
how this access benefits you. Your story matters.

Citation: Foster, John C. et al. "The Impenetrable Barrier: Suppression of Chorus Wave Growth by VLF Transmitters." JGR Space Physics 125, 9 (September 2020): e2020JA027913. © 2020 American Geophysical Union

As Published: <http://dx.doi.org/10.1029/2020ja027913>

Publisher: American Geophysical Union (AGU)

Persistent URL: <https://hdl.handle.net/1721.1/131070>

Version: Final published version: final published article, as it appeared in a journal, conference proceedings, or other formally published context

Terms of Use: Article is made available in accordance with the publisher's policy and may be subject to US copyright law. Please refer to the publisher's site for terms of use.



JGR Space Physics

RESEARCH ARTICLE

10.1029/2020JA027913

Key Points:

- Coherent VLF transmitter signals can entrain resonant electrons at the outer limit of the VLF bubble outside the contracted plasmasphere
- Nonlinear growth of chorus waves and subsequent acceleration of hundreds of keV electrons to MeV energies is suppressed in that region
- Suppression of local MeV acceleration contributes to diffusive and loss-related effects in establishing the impenetrable barrier at $L = 2.8$

Supporting Information:

- Supporting Information S1

Correspondence to:

J. C. Foster,
jcfoster@mit.edu

Citation:

Foster, J. C., Erickson, P. J., Omura, Y., & Baker, D. N. (2020). The impenetrable barrier: Suppression of chorus wave growth by VLF transmitters. *Journal of Geophysical Research: Space Physics*, 125, e2020JA027913. <https://doi.org/10.1029/2020JA027913>

Received 12 FEB 2020

Accepted 2 SEP 2020

Accepted article online 7 SEP 2020

The Impenetrable Barrier: Suppression of Chorus Wave Growth by VLF Transmitters

John C. Foster¹ , Philip J. Erickson¹ , Yoshiharu Omura² , and Daniel N. Baker³ 

¹Haystack Observatory, Massachusetts Institute of Technology, Westford, MA, USA, ²Research Institute for Sustainable Humanosphere, Kyoto University, Kyoto, Japan, ³Laboratory for Atmospheric and Space Physics, University of Colorado Boulder, Boulder, CO, USA

Abstract Rapid radiation belt recovery following storm time depletion involves local acceleration of multi-MeV electrons in nonlinear interactions with VLF chorus waves. Previous studies of an apparent impenetrable barrier at $L \sim 2.8$ focused on diffusion and precipitation loss mechanisms for an explanation of the sharp reduction of multi-MeV electron fluxes earthward of $L \sim 3$. Van Allen Probes observations for cases when the plasmasphere is contracted earthward of $L \sim 3$ indicate that strong coherent signals from VLF transmitters can play significant roles in the suppression of nonlinear chorus wave growth earthward of $L \sim 3$. As a result, local nonlinear acceleration of hundreds of keV electrons to MeV energies does not occur in this region. During the recovery of the outer radiation belt when the plasmasphere is significantly contracted, the suppression of chorus wave growth and local acceleration by the action of the transmitter waves at the outer edge of the VLF bubble contributes to the sharp inner edge of the new MeV electron population and the formation of the impenetrable barrier at $L \sim 2.8$.

Plain Language Summary The variability and intensity of relativistic electrons in Earth's outer radiation belt pose serious space weather concerns. Highly relativistic (MeV) electrons are accelerated locally in rapid nonlinear interactions with very low frequency (VLF) naturally generated rising tone chorus waves. Chorus risers, in turn, grow through interactions with tens of keV electrons injected earthward from the outer magnetosphere during storm conditions. Most of the MeV electrons are lost early in such storms and are seen then to recover rapidly through this local acceleration process. Strong man-made signals from VLF transmitters extend outward in space forming a bubble of wave energy surrounding Earth and confined by its magnetic field. At the outer limits of the bubble, the transmitter waves interact strongly with the tens of keV electrons preventing the growth of the chorus waves that act to accelerate electrons to MeV energies. These effects act to establish a sharp earthward boundary of the rapidly recovering radiation belt MeV electron population at a distance ~ 2.8 Earth radii from our planet. This persistently observed boundary has been termed the impenetrable barrier.

1. Introduction

Dual toroids of energetic protons and electrons circling the Earth were discovered early in the Space Age—the Van Allen radiation belts (Van Allen et al., 1958). Lying earthward of $L \sim 2$, a relatively stable inner zone consists of multi-MeV protons. While fluxes of tens to hundreds of keV electrons can extend into the slot region ($2 < L < 3$), relativistic (> 500 keV), and highly relativistic (> 3 MeV) electrons in the outer radiation belt are typically confined to $L > 3$. The characteristics and dynamics of the multi-MeV electron fluxes are strongly dependent on storm time processes leading to pronounced loss and often rapid recovery of their outer radiation belt populations (e.g., Reeves et al., 2013; Ukhorskiy et al., 2006). As a result, the high-energy outer belt electron fluxes vary significantly in their spatial extent and on multiple time scales.

Nonlinear processes play a significant role in determining the dynamic variability of relativistic electrons in Earth's outer radiation belt. Despite drastic changes in the geomagnetic field configuration during solar storms that result in an almost total depletion of the MeV outer belt electrons, a rapid recovery of the outer zone can subsequently take place in a matter of a few hours (e.g., Baker, Jaynes, Li, et al., 2014). In the following study, we use Van Allen Probes (Mauk et al., 2012) observations to examine intercoupled the roles played by cold plasmaspheric electrons (Electric Field and Waves, EFW; Wygant et al., 2013), keV electrons (Magnetic Electron Ion Spectrometer, MagEIS; Blake et al., 2013), and plasma waves (Electric and Magnetic

Field Instrument and Integrated Science, EMFISIS; Kletzing et al., 2012) in the recovery of multi-MeV electrons (Relativistic Electron-Proton Telescope, REPT; Baker et al., 2012).

Radiation belt recovery in the inner magnetosphere involves local acceleration of hundreds of keV seed electrons to multi-MeV energies in the low-density region outside the plasmapause (Reeves et al., 2013) through interactions with whistler mode very low frequency (VLF) chorus waves (Li et al., 2016; Thorne et al., 2013). Jaynes et al. (2015) have shown that magnetospheric substorm activity produces two distinct electron populations that are essential to the acceleration of highly relativistic electrons in the outer belt: a source population of tens of keV electrons that drive VLF wave growth, and a seed population at hundreds of keV that are then accelerated by the VLF waves to MeV energies. The recovery of multi-MeV electrons at $L \sim 3$ –5 can take place rapidly (30–60 min), indicating the importance of nonlinear processes (Foster et al., 2014). In the following sections we present Van Allen Probes observations that indicate that, for cases where the plasmapause moves strongly inward, strong coherent VLF transmitter signals at the outer edge of a VLF bubble surrounding Earth (Foster et al., 2016) can contribute to the suppression of nonlinear chorus wave growth and local MeV electron acceleration and the formation of a seemingly impenetrable barrier for the occurrence of multi-MeV electrons earthward of $L \sim 2.8$.

2. The Impenetrable Barrier

Baker, Jaynes, Hoxie, et al. (2014) found that highly relativistic (>2 MeV) and ultrarelativistic (>5 MeV) electrons in the outer radiation belt were found at $L \gtrsim 3$ but were not observed at lower L values. Considering that diffusive radial transport and pitch angle diffusion into the loss cone proceed very slowly for relativistic electrons at $2.5 < L < 3$ (Abel & Thorne, 1998), Baker, Jaynes, Hoxie, et al. (2014) theorized that very slow inward radial diffusion combined with loss through weak wave-particle pitch angle scattering were the most likely causes of an apparent barrier for relativistic electrons at the earthward edge of the outer radiation belt near $L = 2.8$.

Ozeke et al. (2018) presented simulations of the action of ultralow frequency wave radial diffusion on the formation of the apparent impenetrable barrier during the recovery phase of geomagnetic storms. Their simulations result in the creation of a very steep radial gradient in flux at the inner edge of the outer ultrarelativistic radiation belt and find that the location of this gradient changes with time and from storm to storm. However, for the period between September 2012 and May 2014 there was no evidence of penetration of ultrarelativistic electron flux inward of $L \sim 2.8$ in the simulation results. They conclude that the apparently impenetrable barrier can be explained naturally by inwards ULF wave radial transport. The overall results of Ozeke et al. (2018) are similar to the initial conclusion reached by Baker, Jaynes, Hoxie, et al. (2014) that the apparent barrier at $L \sim 2.8$ resulted from very slow inward diffusive transport rates around $L \sim 2.8$ in the inner magnetosphere combined with slow wave-particle scattering losses of MeV electrons to the atmosphere due to chorus and plasmaspheric hiss waves.

There are exceptions to the impenetrability of the barrier near $L = 2.8$. In particular, interplanetary shocks can accelerate electrons adiabatically to multi-MeV energies in the inner magnetosphere on a 1 min time scale (Foster et al., 2015), and well inside $L = 2.8$ in extreme cases (Blake et al., 1992). In the absence of subsequent strong disturbances, the initially sharp multi-MeV electron flux boundaries that formed outside $L \sim 2.8$ during the radiation belt recovery from the 17–18 March 2015 storm were observed to diffuse gradually earthward across the barrier to $L \sim 2.5$ over the ensuing months (Baker et al., 2016). The evolution of this boundary for 3.4 MeV REPT electrons is shown in Figure 1b, eventually forming an inner long-lived “storage belt” such as described by Baker et al. (2013).

3. Effects of Anthropogenic VLF Signals

Strong signals at 20–25 kHz from naval VLF frequency radio stations provide one-way communication to submerged submarines. In addressing a possible cause for the impenetrable barrier, Baker, Jaynes, Hoxie, et al. (2014) considered precipitation of energetic electrons through interactions with these transmitter signals. Following on the work of Abel and Thorne (1998), Baker et al. concluded that precipitation loss would only be significant for electrons with energies <0.5 MeV and furthermore would only be important at mid-latitude locations where $L < 2$.

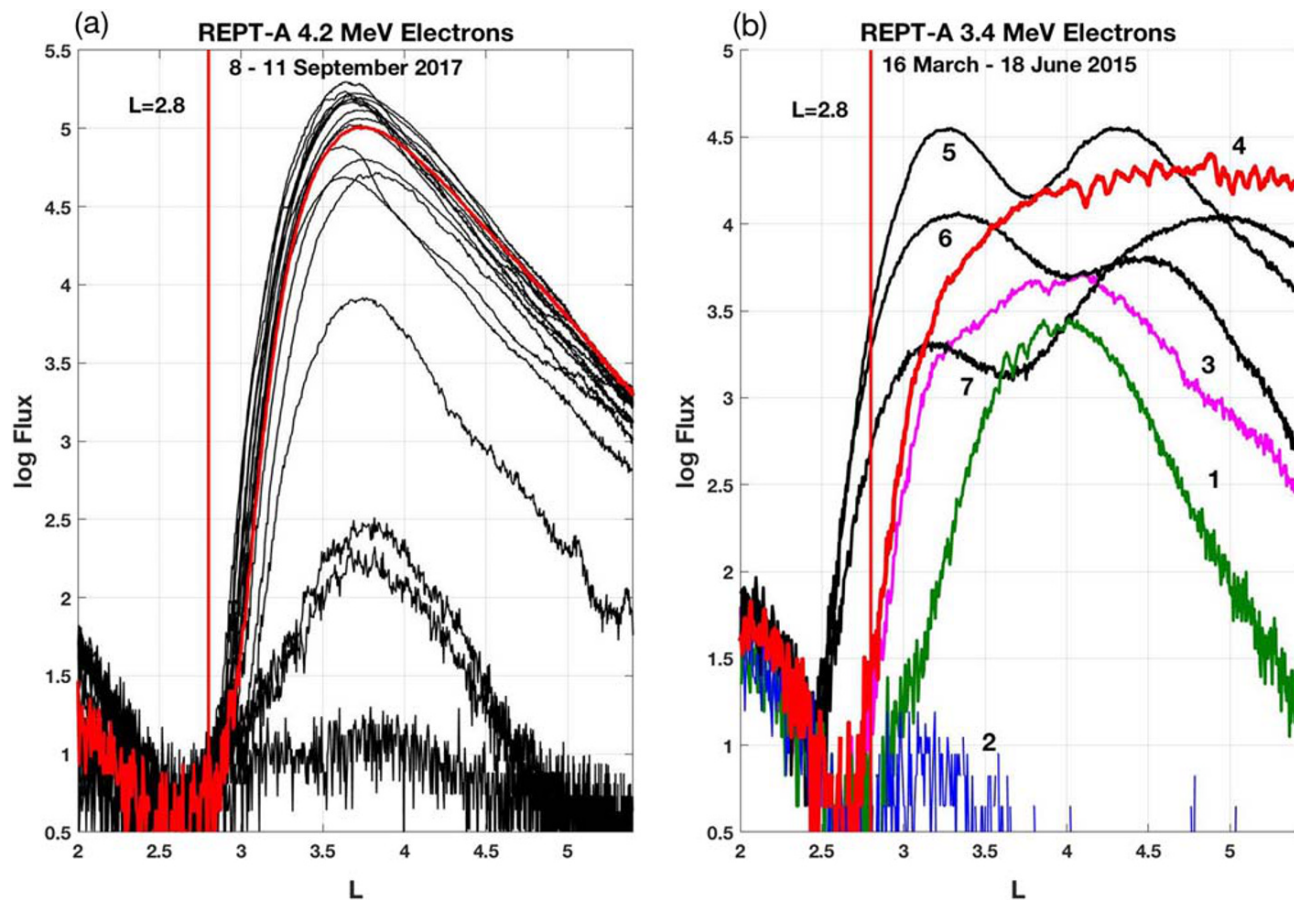


Figure 1. (a) The pass by pass evolution of 4.2 MeV electron flux beginning 8 September 2017 demonstrates the rapid recovery of highly relativistic electrons by >4 orders of magnitude inside $L \sim 4$. Steep gradients were formed outside $L = 2.8$. The red curve highlights the pass at 04:40 UT on 9 September 2017, immediately following the data discussed in Figure 3 (below). (b) The initially sharp multi-MeV electron flux boundaries that formed outside $L = 2.8$ during the 17–18 March 2015 storm gradually diffused earthward across the barrier to $L \sim 2.5$ over the ensuing months. Flux Profiles 1–4 show the evolution of 3.4 MeV fluxes over 24 hr intervals from 16 (1, prestorm) to 19th (4) March. Following storm onset, outer zone fluxes were decreased by $>1,000$ times (2) at $L = 4$. As the outer zone fluxes recovered (3, 4), sharp gradients were formed outside $L = 2.8$. Profiles 5 (18 April), 6 (18 May), and 7 (18 June) show the evolution of the residual “storage belt” fluxes over the ensuing 3 months.

For the 17–18 March 2015 storm event discussed above (cf. Figure 1b), Foster et al. (2016) addressed characteristics of the magnetically confined bubble of VLF wave emissions of terrestrial, human-produced origin that surrounds the Earth. VLF whistler mode signals are confined to L shells such that the wave frequency remains $\leq \frac{1}{2}$ the minimum electron gyrofrequency (f_{ce}) along the field line. The outer limit of the VLF bubble at the strong 25 kHz VLF transmitter frequency closely matches the position of the barrier to the inward extent of multi-MeV radiation belt electrons described by Baker, Jaynes, Hoxie, et al. (2014). Foster et al. (2016) showed an observed 1,000 times increase in VLF electric field amplitude at the transmitter frequency seen outside both the $\frac{1}{2}f_{ce}$ boundary and the plasmopause and attributed this effect to wave growth stimulated by the presence of the transmitter signal. An ample energy source for the amplification of VLF emissions near the transmitter frequency was provided by abundant fluxes of 200 keV electrons that extended well earthward of the MeV electrons. Cyclotron ($n = 1$) interactions leading to VLF wave growth take perpendicular energy from the resonant electrons leading to their precipitation loss to the atmosphere (cf. Foster & Rosenberg, 1976; Inan et al., 2007). A recent statistical and modeling study (Ma et al., 2017) has addressed the crucial role played by VLF waves from transmitters in energetic electron loss at $L < 2.5$. Direct evidence for the precipitation loss of the ~ 100 keV electrons resonant with the VLF transmitter frequency during the 18 March 2015 event reported by Foster et al. (2016) is presented in the supporting information for this paper. Foster et al. (2016) reexamined the effects of observed strong VLF transmitter signals and evidence of wave-wave coupling near $L = 2.8$ on the formation of the impenetrable barrier. The processes identified

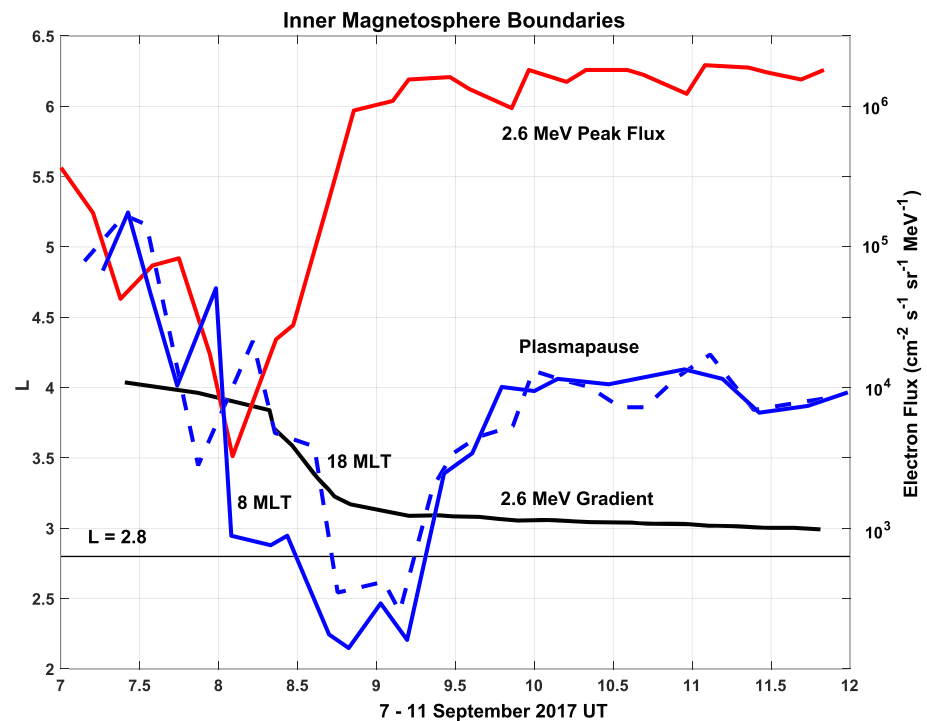


Figure 2. The peak REPT 2.6 MeV electron flux between $L = 3$ and $L = 5$ is indicated by the red curve. The plasmapause (blue curves; electron density $<100 \text{ cm}^{-3}$) was earthward of $L = 3$ during the entire interval of MeV electron recovery. The midpoint of the sharp earthward gradient of 2.6 MeV fluxes (black curve, log flux <4.3) moved inward to $L \sim 3.3$ during the flux recovery. As seen in Figure 1a, MeV electrons were completely excluded inside $L \sim 2.8$.

were calculated to be sufficient to produce enhanced MeV electron precipitation loss in the region beyond the eroded plasmapause significantly greater than that estimated by Baker, Jaynes, Hoxie, et al. (2014).

Both the Baker, Jaynes, Hoxie, et al. (2014) and the Foster et al. (2016) discussions of the impenetrable barrier focused on particle loss mechanisms for an explanation of the sharp reduction of multi-MeV electron fluxes near $L = 2.8$. Baker, Jaynes, Hoxie, et al. (2014) noted that the inner edge of the ultrarelativistic electron population at $L \sim 2.8$ seemed to require that electron acceleration occur just outside that location, since the radial transport of such electrons to $L \sim 2.8$, well inside the nominal position of the plasmapause at $L \sim 4$ – 5 , is usually very slow (years). They concluded that the appearance of robust populations of ultrarelativistic electrons at $L \sim 3$ would require a local wave acceleration process occurring just outside the plasmapause during conditions when the plasmapause was contracted to $L < 3$. In addition, the Foster et al. (2016) study pointed out that, for the March 2015 event, natural chorus band emissions appeared to have been suppressed at the position where the transmitter frequency approached $\frac{1}{2} f_{ce}$ at the edge of the VLF bubble ($L \sim 2.8$).

In this study, we investigate observations for a moderate storm in 2017 when the plasmapause was eroded to $L < 2$. We reconsider the strong VLF transmitter signals observed near $\frac{1}{2} f_{ce}$ at the outer limits of the VLF bubble. Observations and theoretical analysis described below indicate that phase perturbation and subsequent precipitation loss of 10–100 keV electrons in resonance with the growing coherent transmitter signal can result in the suppression of the nonlinear growth of VLF chorus waves. Discrete chorus rising tones are essential for the rapid acceleration of MeV electrons (e.g., Omura, Miyashita, et al., 2015). We suggest that the suppression of local MeV acceleration through the action of the VLF transmitter signal at the outer edge of the VLF bubble can contribute significantly to diffusive and loss-related effects in establishing the impenetrable barrier near $L = 2.8$.

4. Inner Magnetosphere Plasma and Wave Observations

The general characteristics of the 8–9 September 2017 event have been described in detail in the recent literature. A double phase geomagnetic storm on 8 September 2017 (Dst max of -142 and -122 nT,

respectively), combined with multiple solar flare impacts (e.g., Yamauchi et al., 2018), led to a contraction of the plasmasphere, large variations in global total electron content, and unusual midlatitude effects in the plasmasphere boundary layer including deep plasma depletions (Aa et al., 2018). In the outer radiation belt, the event featured a sharp dropout of MeV electron fluxes and their subsequent rapid recovery at L values >2.8 . This is seen in the REPT observations shown in Figure 1a for 4.2 MeV electrons and in Figure 2 (red curve) that shows that the peak REPT 2.6 MeV electron flux between $L = 3$ and $L = 5$ decreased by a factor of 30 at the beginning of 8 September and then increased by 300 times by the beginning of the ninth. Whereas the plasmopause receded to $L \sim 2$ during the strong MeV electron recovery (blue curves), the inward extent of the sharp gradients at the earthward edge of the recovering fluxes formed only outside $L = 2.8$ (black curve). Plasmopause locations at ~ 18 and 08 MLT (density $<100 \text{ cm}^{-3}$; blue curves) were derived from spacecraft potential (EFW) and upper hybrid frequency measurements (EMFISIS).

The propagation of terrestrial VLF signals in the inner magnetosphere has been described by Starks et al. (2009). The primary mode of propagation for $L > \sim 2$ is ducted and restricted to a magnetically confined bubble surrounding Earth at L shells such that the wave frequency is less than $\frac{1}{2}$ the electron cyclotron frequency (f_{ce}). Figure 3a presents the EMFISIS high-frequency (HFR) electric field spectrogram for the inbound pass of RBSP-A at 03:00 UT on 9 September 2017. Strong signals from VLF frequency transmitters (horizontal lines) extend to the outer regions of the VLF bubble. Wave power at the strongest 24.9 kHz transmitter frequency increased by a factor of 10^6 between $L = 3.2$ and $L = 2.7$. In that region, natural whistler mode emissions are suppressed by $\sim 1,000$ times in a band from 20–24 kHz, immediately below the enhanced transmitter frequency. The sharp plasmopause is at $L = 2.1$ at this time and the ratio f_{pe}/f_{ce} is <2 earthward of $L = 2.8$. Close inspection of the HFR spectrum in Figure 3a reveals discrete intense (1,000 times) enhancements of chorus emissions extending into the gap below the transmitter frequency. Whereas the HFR sampling rate is not sufficient to resolve whether these bursts are composed of discrete emissions, the restricted frequency range of these intense emissions to a narrow band below $\frac{1}{2} f_{ce}$ is consistent with the restriction of the onset frequency for nonlinear wave growth in this region of decreased f_{pe}/f_{ce} , as described in section 5 below. This evidence of nonlinear chorus wave growth near $\frac{1}{2} f_{ce}$ ended abruptly inside $L = 2.8$.

The observations presented in Figure 3a for the 9 September 2017 event are qualitatively similar to those discussed by Foster et al. (2016) for the 18 March 2015 storm. In each case natural whistler mode emissions and nonlinear chorus wave growth were suppressed immediately below a strong coherent VLF transmitter signal at the outer extent of the VLF bubble at and around $L = 2.8$.

Naturally generated whistler mode waves experience growth in ($n = 1$) cyclotron interactions with injected electrons (e.g., Foster et al., 1976) through transfer of perpendicular energy from resonant electrons to the waves, driving the electrons toward the precipitation loss cone (e.g., Foster & Rosenberg, 1976). The presence of an anthropogenic, coherent VLF signal in this region also can interact with the same lower-energy electron population. Evidence of such direct interaction of the transmitter signal with lower-energy electrons in the chorus generation region outside the plasmopause is seen in the MagEIS observations across the outer edge of the VLF bubble shown in Figures 3b and 4. The upper panel of Figure 4 presents the variation of the electric field wave power at the 24.9 kHz transmitter frequency across the region. Resonant electron energy at this frequency for the observed conditions was calculated to be ~ 60 keV. Wave power was enhanced >10 times suggesting local amplification of the transmitter signal across the region between the plasmopause and the outer edge of the VLF bubble and was decreased by a factor $>10^5$ outside that region. In the region of transmitter wave power enhancement, the flux of resonant low energy electrons between 30 and 90 keV was decreased by ~ 3 times. These observations are consistent with loss cone scattering of the 10–100 keV electrons resonant with the enhanced transmitter signal. In the same region, subrelativistic electron flux (235 keV) was increased 3 times at perpendicular pitch angles. The local acceleration of relativistic electrons (597 and 1,079 keV) exhibited a sharp flux decrease by factors of 100 inside $L = 3.2$. These interrelated observations indicate that in the region at the outer extent of the VLF bubble where lower-energy injected electrons interacted directly with the transmitter signal, the transmitter wave power grew while nonlinear chorus wave development and MeV acceleration were suppressed.

For the 9 September 2017 event, the MagEIS electron energy range and pitch angle coverage needed to show precipitation loss of the resonant electrons was not available in either the RBSP-A or RBSP-B observations. However, for the very similar barrier event on 18 March 2015, Figure 4b of the earlier Foster et al. (2016)

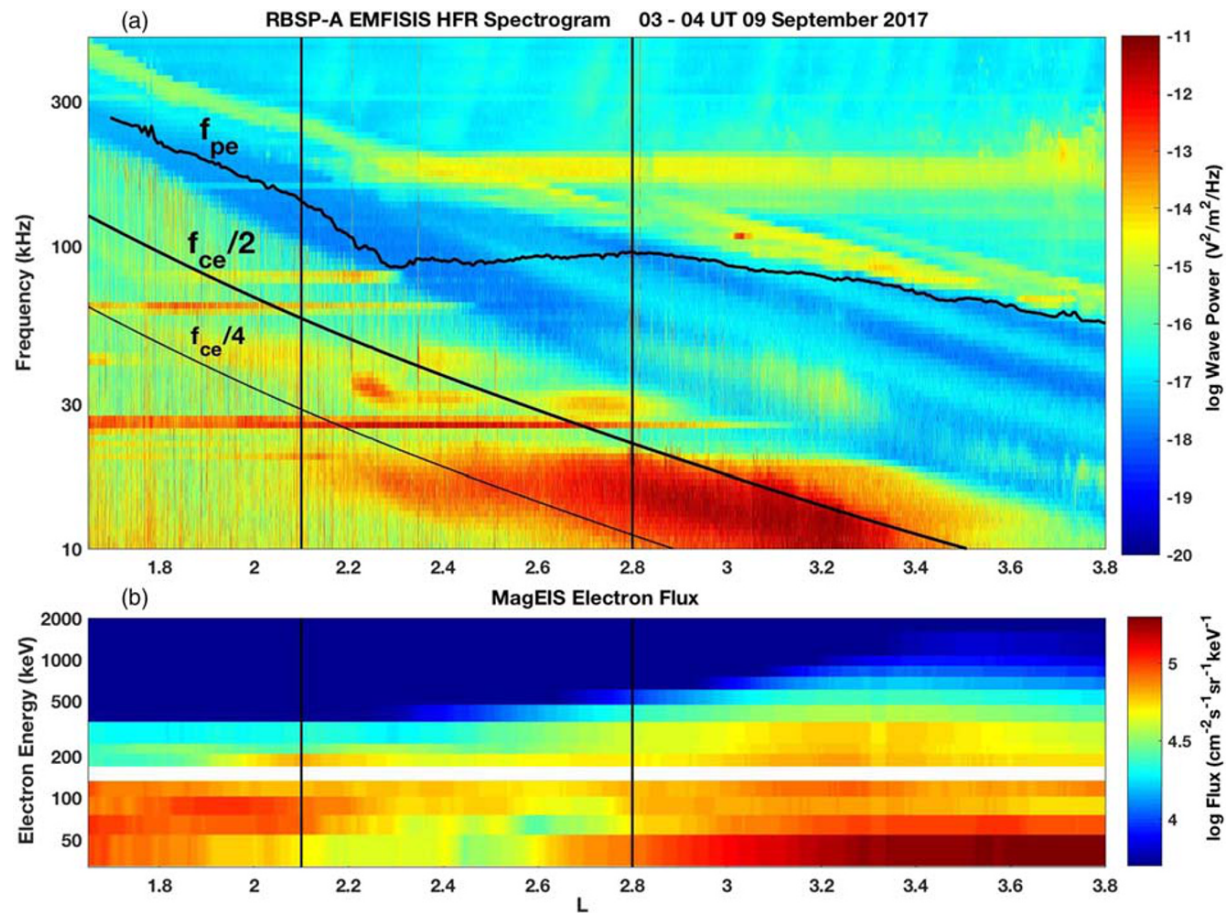


Figure 3. (a) EMFISIS HFR electric field spectrogram for the inbound pass of RBSP-A at 03:00 UT on 9 September 2017. Black vertical lines indicate $L = 2.8$ and $L = 2.1$ (the position of the plasmopause at this time), and heavy black curves show the electron plasma frequency (f_{pe}) and $\frac{1}{2}f_{ce}$. Natural whistler mode emissions are suppressed by $\sim 1,000$ times in a band from 20–24 kHz immediately below the strong VLF transmitter signal at 24.9 kHz. (b) Low energy (<100 keV) MagEIS electron fluxes, measured on a preceding pass of RBSP-B, were depleted between $L = 2.1$ and $L = 2.8$. Electron energies in this range are in cyclotron resonance ($n = 1$) at low pitch angles with VLF waves at the 24.9 kHz transmitter frequency.

study showed that 50–300 keV electrons were resonant with the transmitter frequency at low pitch angles. For that event, RBSP-A MagEIS directly observed loss cone fluxes of the resonant electrons. Those data are presented in the supporting information for this paper.

5. Suppression of Nonlinear Chorus Wave Growth at $L < 2.8$

Initially, whistler waves grow linearly, becoming coherent as the wave grows at the frequency of the largest linear growth rate while also suppressing the growth of other waves around that frequency. When the wave amplitude exceeds a threshold amplitude for nonlinear instability, the wave amplitude grows rapidly as the frequency increases monotonically (Omura et al., 2009). Nonlinear growth stops near the optimum wave amplitude (Omura & Nunn, 2011) and then decreases gradually, forming a discrete subpacket within the chorus rising tone. However, this natural sequence of chorus wave development and subsequent nonlinear relativistic acceleration in the inner magnetosphere can be broken by several interrelated effects, which can occur during unusual storm time plasmasphere configurations.

In the inner magnetosphere the magnetic field strength and f_{ce} increase rapidly with decreasing L . At times when the plasmopause contracts earthward of $L \sim 3$, as in the 9 September 2017 case discussed above, the unusually low plasma density in the inner magnetosphere can alter the conditions needed for nonlinear chorus wave growth, as these are highly dependent on the ratio f_{pe}/f_{ce} of cold plasma frequency to electron cyclotron frequency. Figure 5 presents the results of theoretical calculations (Omura, Nakamura, et al., 2015)

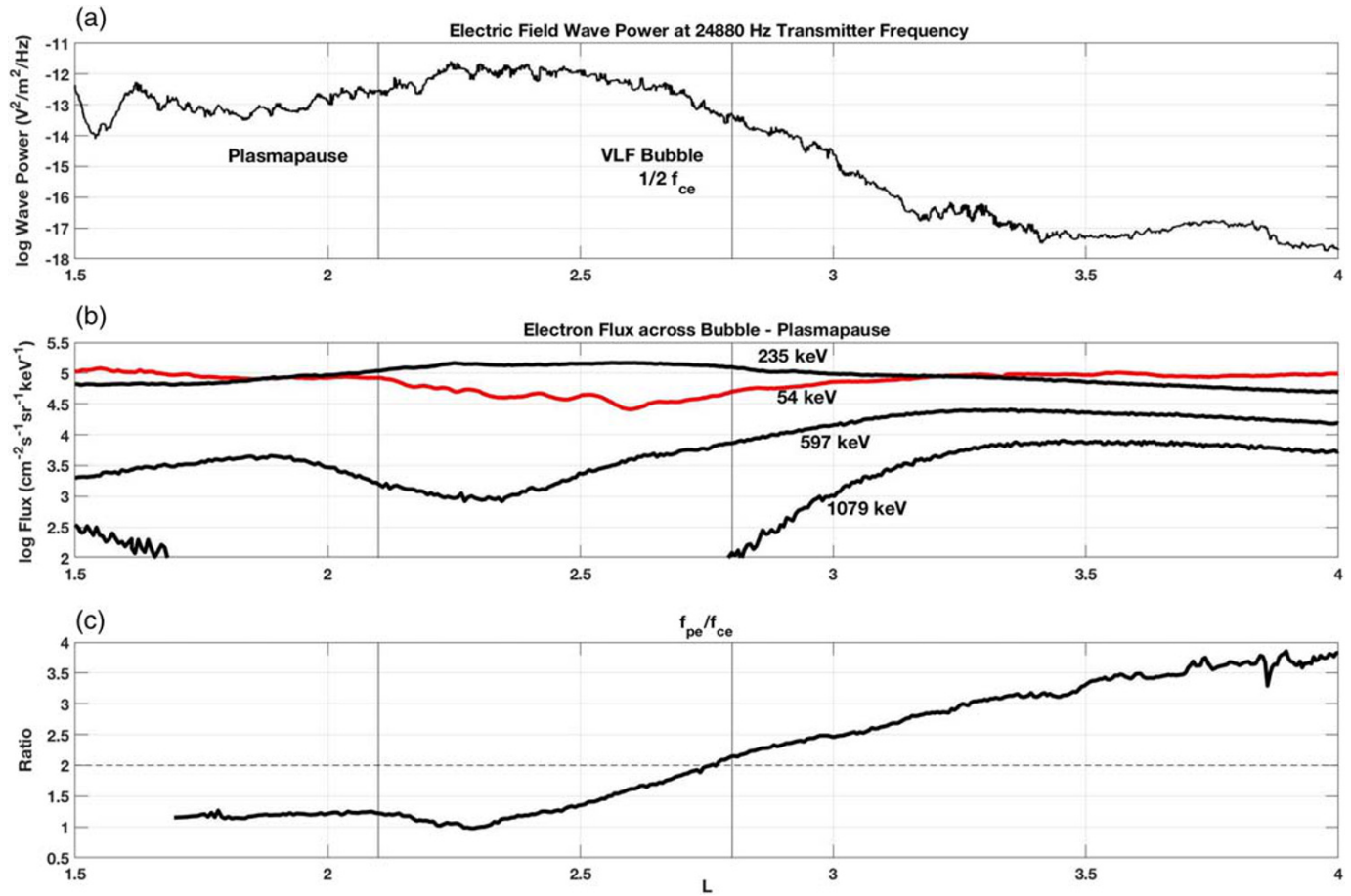


Figure 4. (a) Electric field wave power at the 24.9 kHz transmitter frequency increased by 10 times outside the plasmapause. Black vertical lines indicate $L = 2.1$ and $L = 2.8$. (b) For the pass at ~03:00 on 9 September 2017, the MagEIS 235 keV electron flux (the lowest energy available from RBSP-A at the time) is enhanced between $L = 2.8$ and $L = 2.1$ across the region of the transmitter wave enhancement. The 54 keV electron flux observed by RBSP-B ~3 hr earlier (red curve, cf. Figure 3b) decreased by ~3 times across the region of transmitter wave enhancement. (c) For the event shown in Figure 3, the observed ratio of the plasma frequency to the cyclotron frequency varied from 1 to 3 across the region of transmitter wave enhancement.

that describe the dependencies of the nonlinear threshold frequency and optimum wave amplitude on f_{pe}/f_{ce} . Dashed curves indicate the threshold amplitude for the onset of nonlinear growth as a function of normalized wave frequency ($f_{\text{wave}}/f_{ce} = 0.5$ and 0.25 are indicated by a dotted black line). Solid curves indicate the optimum amplitude for the nonlinear wave growth. Threshold and optimum amplitude curves are shown for three values of f_{pe}/f_{ce} . In the case we are describing, $f_{pe}/f_{ce} \sim 1$ at the location where the VLF transmitter frequency matches $1/2 f_{ce}$ (cf. Figure 4c).

For the results of the Omura, Nakamura, et al. (2015) calculations shown in Figure 5a, f_{pe}/f_{ce} varies as $[3, 2, 1]$ (magenta, blue, and green). The ratio of hot to cold electron densities ($n_h/n_c = 4 \times 10^{-4}$), and the velocity distribution function has been set so that the resonance energy is 40–60 keV (this is specified by parameters in Equation (1) in Hikishima et al., 2010, $U^{\parallel} = 0.23c$, $U^{\perp} = 0.25c$, $\beta = 0.3$, $Q = 0.5$). These calculations show that in a region where the cold plasma density (n_c) is low enough such $f_{pe}/f_{ce} \sim 1$, the nonlinear threshold amplitude exceeds the optimum (maximum) amplitude for wave growth at $L \sim 2.8$, totally suppressing the development of chorus rising tones.

A complementary effect is the suppression of the chorus wave growth in the presence of a strong coherent transmitter signal near the chorus wave starting frequency. The strong constant frequency transmitter signal can entrain the resonant electrons suppressing the development of rising tone emissions. Wave power grows at the transmitter frequency and resonant electrons in the 50–100 keV range are lost by precipitation. Strong

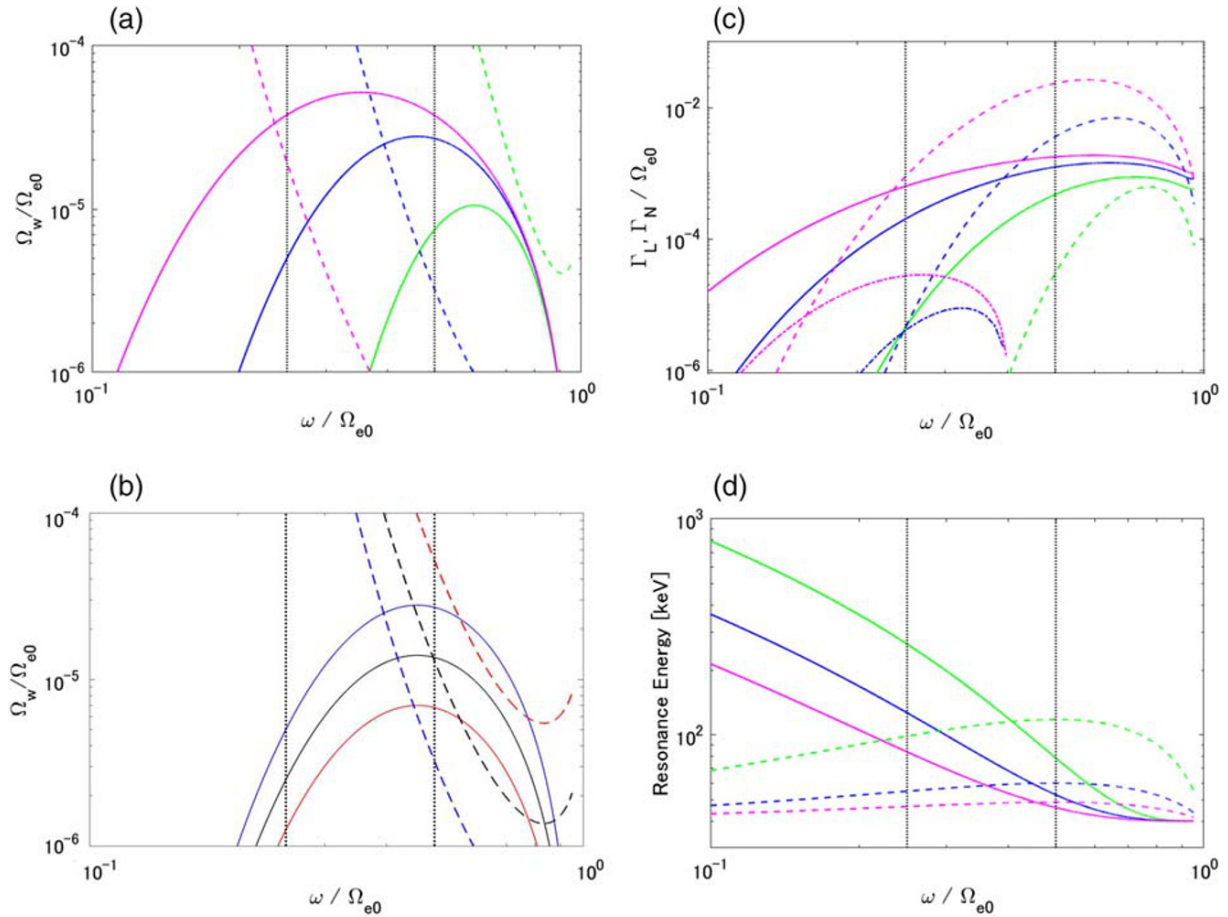


Figure 5. (a) Optimum amplitudes (solid line) and threshold amplitudes (dashed line) for different ratios $f_{pe}/f_{ce} = [3, 2, 1]$ (magenta, blue, green) with $n_h/n_c = 4 \times 10^{-4}$. (b) Optimum amplitudes (solid line) and threshold amplitudes (dashed line) for different $n_h/n_c = [4, 2, 1] \times 10^{-4}$ (blue, black, and red) with $f_{pe}/f_{ce} = 2$. (c) Linear growth rates (dash-dotted line), nonlinear growth rates at threshold amplitudes (dashed line), and nonlinear growth rates at optimum amplitudes (solid line) for different $f_{pe}/f_{ce} = [3, 2, 1]$ (magenta, blue, and green) with $n_h/n_c = 4 \times 10^{-4}$. (d) Resonance energies of cyclotron resonance (solid line) and Landau resonance ($n = 0$) at quasi-parallel propagation (dashed line) for different $f_{pe}/f_{ce} = [3, 2, 1]$ (magenta, blue, and green) with $n_h/n_c = 4 \times 10^{-4}$.

evidence of the direct interaction of the transmitter signal with these lower-energy electrons has been presented in the flux “bite-out” seen in the MagEIS observations as shown in Figures 3b and 4.

Precipitation loss of tens to 100 keV electrons resonant with the enhanced transmitter waves was seen in MagEIS pitch angle observations during the 18 March 2015 event (cf. Figure 1b) and is included here in the supporting information. Figure 5b demonstrates the effect of the depletion of the resonant electrons (n_h) by the transmitter wave. We vary n_h/n_c as 1×10^{-4} , 2×10^{-4} , and 4×10^{-4} (red, black, and blue curves), while other parameters are the same ($f_{pe}/f_{ce} = 2$). As the density of hot resonant electrons decreases (blue \rightarrow black \rightarrow red), the overlap of the optimum and threshold amplitudes decreases and disappears. The decrease in density of the hot electrons around the resonant energy caused by their interactions with the transmitter signal prevents the development of the chorus waves responsible for local MeV electron acceleration. The resonant electron energy is determined from the resonance condition which depends on the ratio of f_{pe}/f_{ce} especially in the low-frequency range. As shown in Figure 5d, the ($n = 1$) resonance energy becomes higher with lower f_{pe}/f_{ce} . Since the flux of the resonant electrons decreases for higher energy, generation of chorus emissions becomes unlikely at lower L . Linear and nonlinear growth rates for $f_{pe}/f_{ce} = 1, 2$, and 3 are plotted in Figure 5c. The linear growth rate for $f_{pe}/f_{ce} = 1$ (green) is 0 or negative and does not appear in the logarithmic scale of Figure 5c, while the nonlinear growth rates are much greater than the linear growth rates.

The absence of chorus development prevents the local acceleration of hundreds of keV seed electrons to relativistic energies. During the recovery of the outer radiation belt when the plasmasphere is significantly

contracted, the suppression of chorus wave growth and local acceleration by the rapid decrease of f_{pe}/f_{ce} combined with the action of the transmitter waves on resonant electrons at the outer edge of the VLF bubble can contribute significantly to the formation of a sharp inner edge of the new MeV electron population and the appearance of a seemingly impenetrable barrier at $L \sim 2.8$.

6. Discussion

Foster et al. (2017), Hsieh and Omura (2018), and Omura et al. (2019) have presented the theory for nonlinear wave-particle electron acceleration in interactions with strong chorus rising tones outside the plasmopause and have applied these calculations to Van Allen Probes observations during rapid radiation belt recovery events. Nonlinear acceleration by strong VLF chorus rising tones is sufficient to explain the prompt (30–60 min) increase of multi-MeV electron fluxes in the inner magnetosphere by factors of tens to 100 as reported by Foster et al. (2014). A localized set of processes near $L \sim 3$ that suppresses the development of chorus rising tones would produce a sharp earthward boundary of the region of multi-MeV local electron acceleration and flux enhancement that Baker, Jaynes, Hoxie, et al. (2014) have described as the impenetrable barrier. Near $L \sim 3$ in the low-density region outside the plasmopause the ratio f_{pe}/f_{ce} is decreasing rapidly and the nonlinear starting frequency of the chorus emission is shifted to the ~ 25 kHz frequency of strong VLF transmitter signals. Interaction with the strong coherent transmitter wave leads to the precipitation of resonant electrons and a reduction of the hot/cold electron density ratio, leading to the suppression of nonlinear chorus development. In the absence of chorus rising tones, the local acceleration of electrons to MeV energies is shut down at the outer edge of the VLF bubble creating an apparent impenetrable barrier to their earthward extent. Because of the very slow cross- L diffusion for MeV electrons inside $L = 3$ (e.g., Baker, Jaynes, Hoxie, et al., 2014; Ozeke et al., 2018), the sharp earthward flux gradients formed outside the region of chorus suppression can persist for days to weeks without extending significantly earthward of $L \sim 2.8$.

7. Summary

For conditions when the plasmasphere is contracted inside $L \sim 2.8$, two factors combine to suppress local acceleration of hundreds of keV seed electrons to relativistic energies at $L < 3$. (1) The ratio of f_{pe}/f_{ce} decreases to values < 2 in the low-density region outside the plasmopause where the magnetic field strength increases rapidly with decreasing L . (2) Interaction of resonant electrons with the VLF transmitter waves decreases the hot tens to 100 keV electron population (n_h) needed to support nonlinear chorus wave growth. The calculations of Figure 5 indicate that, for the circumstances observed, a suppression of the nonlinear growth of chorus waves near $L \sim 2.8$ would result both from the localized decrease in f_{pe}/f_{ce} and the reduction of the density of the gyroresonant electron population. In the absence of chorus rising tones, the rapid nonlinear acceleration of electrons to MeV energies earthward of $L \sim 3$ is suppressed. The result is an abrupt, sharp inner edge of the newly created MeV electron population and the appearance of an impenetrable barrier at the fixed location where the strongest transmitter signals near 25 kHz cross $\frac{1}{2}f_{ce}$ at the outer extent of the VLF bubble at $L \sim 2.8$.

Data Availability Statement

Van Allen Probes observations used in this study can be obtained through instrument websites (EMFISIS wave data: <http://emfisis.physics.uiowa.edu>; MageIS and REPT particle data: https://rbsp-ect.lanl.gov/rbsp_ect.php; EFW data: <http://www.space.umn.edu/rbsp-efw-data/>). The values of the optimum and threshold amplitudes in Figures 5a and 5b are calculated by Equations (29) and (35) in Omura, Nakamura, et al. (2015). The nonlinear growth rates are calculated by Equation (22) in Omura et al. (2009), and the linear growth rates are obtained by KUPDAP (Sugiyama et al., 2015; <http://space.rish.kyoto-u.ac.jp/software/>).

References

- Aa, E., Huang, W., Liu, S., Ridley, A., Zou, S., Shi, L., et al. (2018). Midlatitude plasma bubbles over China and adjacent areas during a magnetic storm on 8 September 2017. *Space Weather*, 16, 321–331. <https://doi.org/10.1002/2017SW001776>
- Abel, B., & Thorne, R. M. (1998). Electron scattering loss in Earth's inner magnetosphere 1. Dominant physical processes. *Journal of Geophysical Research*, 103(A2), 2385–2396. <https://doi.org/10.1029/97JA02919>

Acknowledgments

This research was supported by the NASA Van Allen Probes (RBSP) funding provided under NASA prime Contract NAS5-01072, including the EFW investigation (PI: J. R. Wygant, University of Minnesota), and the ECT investigation (PI: H. Spence, University of New Hampshire). The work at Kyoto University is supported by JSPS KAKENHI Grant 17H06140.

- Baker, D. N., Jaynes, A. N., Hoxie, V. C., Thorne, R. M., Foster, J. C., Li, X., et al. (2014). An impenetrable barrier to ultrarelativistic electrons in the Van Allen radiation belts. *Nature*, 515(7528), 531–534. <https://doi.org/10.1038/nature13956>
- Baker, D. N., Jaynes, A. N., Kanekal, S. G., Foster, J. C., Erickson, P. J., Fennell, J. F., et al. (2016). Highly relativistic radiation belt electron acceleration, transport, and loss: Large solar storm events of March and June 2015. *Journal of Geophysical Research: Space Physics*, 121, 6647–6660. <https://doi.org/10.1002/2016JA022502>
- Baker, D. N., Jaynes, A. N., Li, X., Henderson, M. G., Kanekal, S. G., Reeves, G. D., et al. (2014). Gradual diffusion and punctuated phase space density enhancements of highly relativistic electrons: Van Allen Probes observations. *Geophysical Research Letters*, 41, 1351–1358. <https://doi.org/10.1002/2013GL058942>
- Baker, D. N., Kanekal, S. G., Hoxie, V. C., Batiste, S., Bolton, M., Li, X., et al. (2012). The Relativistic Electron-Proton Telescope (REPT) instrument on board the Radiation Belt Storm Probes (RBSP) spacecraft: Characterization of Earth's radiation belt high-energy particle populations. *Space Science Reviews*, 179(1–4), 337–381. <https://doi.org/10.1007/s11214-012-9950-9>
- Baker, D. N., Kanekal, S. G., Hoxie, V. C., Henderson, M. G., Li, X., Spence, H. E., et al. (2013). A long-lived relativistic electron storage ring embedded in Earth's outer Van Allen belt. *Science*, 340(6129), 186–190. <https://doi.org/10.1126/science.1233518>
- Blake, J. B., Carranza, P. A., Claudepierre, S. G., Clemmons, J. H., Crain, W. R. Jr., Dotan, Y., et al. (2013). Magnetic Electron Ion Spectrometer (MagEIS) instruments aboard the Radiation Belt Storm Probes (RBSP) spacecraft. *Space Science Reviews*, 179(1–4), 383–421. <https://doi.org/10.1007/s11214-013-9991-8>
- Blake, J. B., Kolasinski, W. A., Fillius, R. W., & Mullen, E. G. (1992). Injection of electrons and protons with energies of 10s of MeV into $L < 3$ on March 24, 1991. *Geophysical Research Letters*, 19, 821. <https://doi.org/10.1029/92gl00624>
- Foster, J. C., Erickson, P. J., Baker, D. N., Claudepierre, S. G., Kletzing, C. A., Kurth, W., et al. (2014). Prompt energization of relativistic and highly relativistic electrons during substorm intervals: Van Allen Probes observations. *Geophysical Research Letters*, 41, 20–25. <https://doi.org/10.1002/2013GL058438>
- Foster, J. C., Erickson, P. J., Baker, D. N., Jaynes, A. N., Mishin, E. V., Fennell, J. F., et al. (2016). Observations of the impenetrable barrier, the plasmopause, and the VLF bubble during the 17 March 2015 storm. *Journal of Geophysical Research: Space Physics*, 121, 5537–5548. <https://doi.org/10.1002/2016JA022509>
- Foster, J. C., Erickson, P. J., Omura, Y., Baker, D. N., Kletzing, A., & Claudepierre, S. G. (2017). Van Allen Probes observations of prompt MeV radiation belt electron acceleration in nonlinear interactions with VLF chorus. *Journal of Geophysical Research: Space Physics*, 122, 324–339. <https://doi.org/10.1002/2016JA023429>
- Foster, J. C., & Rosenberg, T. J. (1976). Electron precipitation and VLF emissions associated with cyclotron resonance interactions near the plasmopause. *Journal of Geophysical Research*, 81(13), 2183–2192. <https://doi.org/10.1029/JA081i013p02183>
- Foster, J. C., Rosenberg, T. J., & Lanzerotti, L. J. (1976). Magnetospheric conditions at the time of enhanced wave-particle interactions near the plasmopause. *Journal of Geophysical Research*, 81(13), 2175–2182. <https://doi.org/10.1029/JA081i013p02175>
- Foster, J. C., Wygant, J. R., Hudson, M. K., Boyd, A. J., Baker, D. N., Erickson, P. J., & Spence, H. E. (2015). Shock-induced prompt relativistic electron acceleration in the inner magnetosphere. *Journal of Geophysical Research: Space Physics*, 120, 1661–1674. <https://doi.org/10.1002/2014JA020642>
- Hikishima, M., Omura, Y., & Summers, D. (2010). Self-consistent particle simulation of whistler mode triggered emissions. *Journal of Geophysical Research*, 115, A12246. <https://doi.org/10.1029/2010JA015860>
- Hsieh, Y.-K., & Omura, Y. (2018). Nonlinear damping of oblique whistler mode waves via Landau resonance. *Journal of Geophysical Research: Space Physics*, 123, 7462–7472. <https://doi.org/10.1029/2018JA025848>
- Inan, U. S., Piddychiy, D., Peter, W. B., Sauvaud, J. A., & Parrot, M. (2007). DEMETER satellite observations of lightning-induced electron precipitation. *Geophysical Research Letters*, 34, L07103. <https://doi.org/10.1029/2006GL029238>
- Jaynes, A. N., Baker, D. N., Singer, H. J., Rodriguez, J. V., Loto'aniu, T. M., Ali, A. F., et al. (2015). Source and seed populations for relativistic electrons: Their roles in radiation belt changes. *Journal of Geophysical Research: Space Physics*, 120, 7240–7254. <https://doi.org/10.1002/2015JA021234>
- Kletzing, C. A., Kurth, W. S., Acuna, M., MacDowall, R. J., Torbert, R. B., Averkamp, T., et al. (2012). The Electric and Magnetic Field Instrument and Integrated Science (EMFISIS) on RBSP. *Space Science Reviews*, 179(1–4), 127–181. <https://doi.org/10.1007/s11214-013-9993-6>
- Li, W., Ma, Q., Thorne, R. M., Bortnik, J., Zhang, X. J., Li, J., et al. (2016). Radiation belt electron acceleration during the 17 March 2015 geomagnetic storm: Observations and simulations. *Journal of Geophysical Research: Space Physics*, 121, 5520–5536. <https://doi.org/10.1002/2016JA022400>
- Ma, Q., Mourenas, D., Li, W., Artemyev, A., & Thorne, R. M. (2017). VLF waves from ground-based transmitters observed by the Van Allen Probes: Statistical model and effects on plasmaspheric electrons. *Geophysical Research Letters*, 44, 6483–6491. <https://doi.org/10.1002/2017GL073885>
- Mauk, B. H., Fox, N. J., Kanekal, S. G., Kessel, R. L., Sibeck, D. G., & Ukhorskiy, A. (2012). Science objectives and rationale for the Radiation Belt Storm Probes mission. *Space Science Reviews*, 179(1–4), 3–27. <https://doi.org/10.1007/s11214-012-9908-y>
- Omura, Y., Hikishima, M., Katoh, Y., Summers, D., & Yagitani, S. (2009). Nonlinear mechanisms of lower-band and upper-band VLF chorus emissions in the magnetosphere. *Journal of Geophysical Research*, 114, A07217. <https://doi.org/10.1029/2009JA014206>
- Omura, Y., Hsieh, Y.-K., Foster, J. C., Erickson, P. J., Kletzing, C. A., & Baker, D. N. (2019). Cyclotron acceleration of relativistic electrons through Landau resonance with obliquely propagating whistler mode chorus emissions. *Journal of Geophysical Research: Space Physics*, 124, 2795–2810. <https://doi.org/10.1029/2018JA026374>
- Omura, Y., Miyashita, Y., Yoshikawa, M., Summers, D., Hikishima, M., Ebihara, Y., & Kubota, Y. (2015). Formation process of relativistic electron flux through interaction with chorus emissions in the Earth's inner magnetosphere. *Journal of Geophysical Research: Space Physics*, 120, 9545–9562. <https://doi.org/10.1002/2015JA021563>
- Omura, Y., Nakamura, S., Kletzing, C. A., Summers, D., & Hikishima, M. (2015). Nonlinear wave growth theory of coherent hiss emissions in the plasmasphere. *Journal of Geophysical Research: Space Physics*, 120, 7642–7657. <https://doi.org/10.1002/2015JA021520>
- Omura, Y., & Nunn, D. (2011). Triggering process of whistler mode chorus emissions in the magnetosphere. *Journal of Geophysical Research: Space Physics*, 116, A05205. <https://doi.org/10.1029/2010ja016280>
- Ozeke, L. G., Mann, I. R., Murphy, K. R., Degeling, A. W., Claudepierre, S. G., & Spence, H. E. (2018). Explaining the apparent impenetrable barrier to ultra-relativistic electrons in the outer Van Allen belt. *Nature Communications*, 9(1), 1844. <https://doi.org/10.1038/s41467-018-04162-3>
- Reeves, G. D., Spence, H. E., Henderson, M. G., Morley, S. K., Friedel, R. H. W., Funsten, H. O., et al. (2013). Electron acceleration in the heart of the Van Allen radiation belts. *Science*, 341(6149), 991–994. <https://doi.org/10.1126/science.1237743>

- Starks, M. J., Bell, T. F., Quinn, R. A., Inan, U. S., Piddyachiy, D., & Parrot, M. (2009). Modeling of Doppler-shifted terrestrial VLF transmitter signals observed by DEMETER. *Geophysical Research Letters*, *36*, L12103. <https://doi.org/10.1029/2009GL038511>
- Sugiyama, H., Singh, S., Omura, Y., Shoji, M., Nunn, D., & Summers, D. (2015). Electromagnetic ion cyclotron waves in the Earth's magnetosphere with a kappa-Maxwellian particle distribution. *Journal of Geophysical Research: Space Physics*, *120*, 8426–8439. <https://doi.org/10.1002/2015JA021346>
- Thorne, R. M., Li, W., Ni, B., Ma, Q., Bortnik, J., Chen, L., et al. (2013). Rapid local acceleration of relativistic radiation-belt electrons by magnetospheric chorus. *Nature*, *504*(7480), 411–414. <https://doi.org/10.1038/nature12889>
- Ukhorskiy, A. Y., Anderson, B. J., Brandt, P. C., & Tsyganenko, N. A. (2006). Storm time evolution of the outer radiation belt: Transport and losses. *Journal of Geophysical Research*, *111*, A11S03. <https://doi.org/10.1029/2006JA011690>
- Van Allen, J. A., Ludwig, G. H., Ray, E. C., & McIlwain, C. E. (1958). Observation of high intensity radiation by satellites 1958 alpha and gamma. *Jet Propulsion*, *28*(9), 588–592. <https://doi.org/10.2514/8.7396>
- Wygant, J. R., Bonnell, J. W., Goetz, K., Ergun, R. E., Mozer, F. S., Bale, S. D., et al. (2013). The Electric Field and Waves (EFW) instruments on the Radiation Belt Storm Probes Mission. *Space Science Reviews*, *179*(1–4), 183–220. <https://doi.org/10.1007/s1124-013-0013-7>
- Yamauchi, M., Sergienko, T., Enell, C.-F., Schillings, A., Slapak, R., Johnsen, M. G., et al. (2018). Ionospheric response observed by EISCAT during the 6–8 September 2017 space weather event: Overview. *Space Weather*, *16*, 1437–1450. <https://doi.org/10.1029/2018SW001937>

The Impenetrable Barrier: Suppression of Chorus Wave Growth by VLF Transmitters

John C. Foster¹, Philip J. Erickson¹, Yoshiharu Omura² and Daniel N. Baker³

¹ MIT Haystack Observatory, Westford, Massachusetts, USA

² Research Institute for Sustainable Humanosphere, Kyoto University, Kyoto, Japan

³ Laboratory for Atmospheric and Space Physics, University of Colorado, Boulder, Colorado, USA

Contents of this file

Text S1

Figures S1,S2

Introduction

The Foster et al. (2016) study of the prompt recovery of multi-MeV electron fluxes immediately outside $L \sim 2.8$ during the March 17-18, 2015 event (c.f. Figure 1a) described conditions and effects markedly similar to those observed on 09 September 2017. These included contraction of the plasmopause earthward of $L=2.8$, strong (1000x) enhancement of the 21.5 kHz transmitter signal at the outer edge of the VLF bubble, and suppression of risers and other natural whistler-mode emissions at frequencies immediately below the enhanced transmitter signal. Here we present MagEIS low energy electron observations for the March 18, 2015 event that indicate the precipitation of resonant electrons spatially localized with the enhancement of the transmitter signal.

Text S1.

For the 09 Sept. 2017 event, the MagEIS electron energy channels and pitch angle coverage needed to show precipitation loss for electrons resonant at the transmitter frequency were not provided by either RBSP-A or B. However, for the event on 18 March 2015 reported by Foster et al. (2016), the electron energies resonant with the transmitter frequency at low pitch angles (50-300 keV) were well observed by MagEIS-A. For that event, Figure S1 shows an enhancement of

the transmitter signal beyond the plasmopause and a localized decrease in the fluxes of resonant electrons similar to those presented in Figure 4 (panels a and b) in the main text. Figure S2 presents MagEIS-A electron energy / pitch angle distributions indicating resonant-energy (~ 100 keV) electron precipitation across the region of VLF transmitter signal enhancement ($L = 2.6$ to $L = 3.1$). Pitch angle measurements 0 - 150 deg were available across the L range of interest and electron flux enhancements in the lowest pitch angle bin were confined to the region of transmitter wave power enhancement.

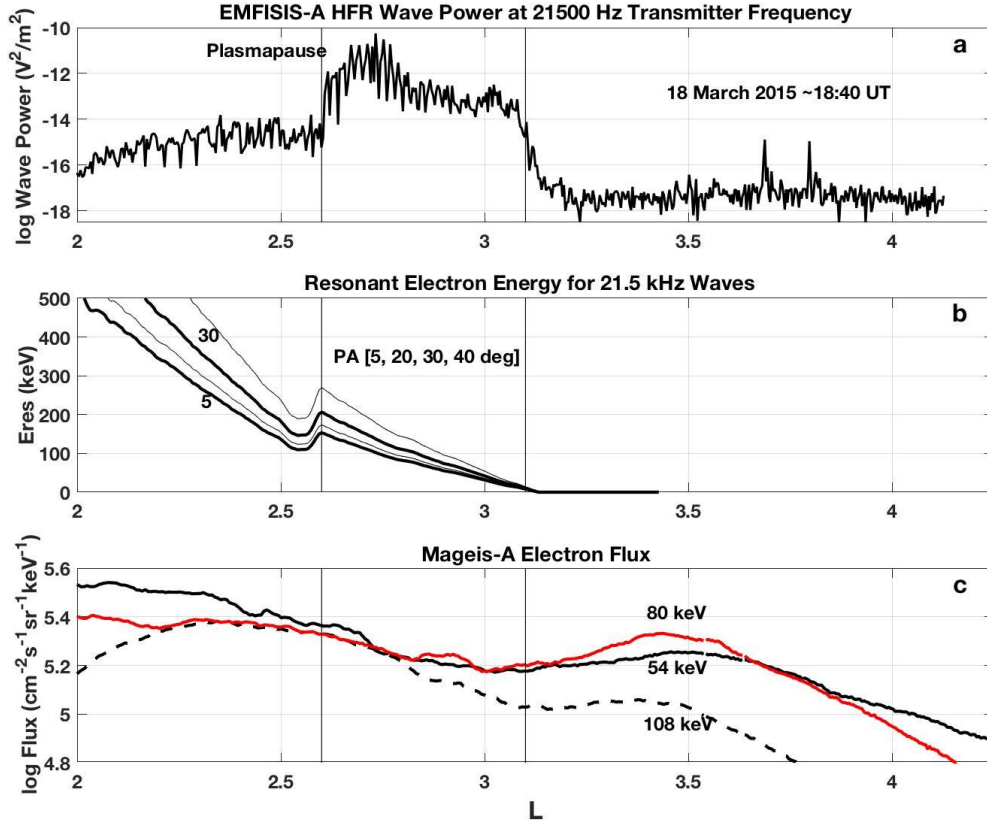


Figure S1. (a) Transmitter wave power increased 1000x across the outer edge of the VLF bubble. The plasmopause was at $L \sim 2.6$ at this time during the 18 March 2015 event (from Foster et al., 2016).

(b) Cyclotron ($n = 1$) resonant energy with 21.5 kHz waves (10 deg wave normal angle) are shown for electrons with pitch angles < 40 deg. Resonant energy was calculated using the observed profiles of electron density and magnetic field strength.

(c) MagEIS electron flux profiles at energies resonant at 21.5 kHz across the region of transmitter wave enhancement outside the plasmopause.

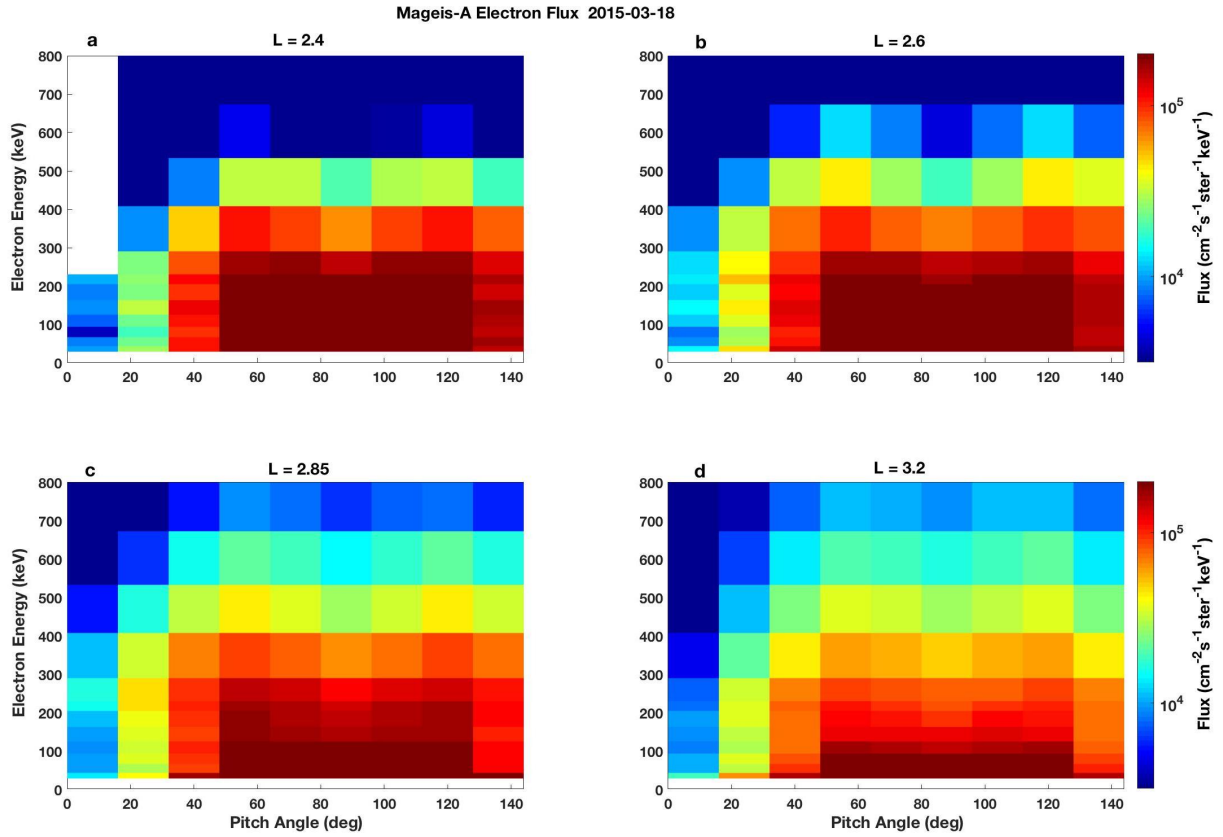


Figure S2. For the 18 March 2015 event, MagEIS-A electron pitch angle distributions at 4 values of L are shown in panels a - d. Precipitation of ~ 100 keV resonant electrons was observed (panels b & c) in the region of transmitter wave enhancement outside the plasmopause at $L = 2.6$ (cf. Figure S1).